High regional climate sensitivity over continental China constrained by glacial-recent changes in temperature and the hydrological cycle

Robert A. Eagle[a,b,1], Camille Risi[c,d], Jonathan L. Mitchell[a,e], John M. Eiler[b], Ulrike Seibt[a,e], J. David Neelin[e,f], Gaojun Li[g], and Aradhna K. Tripati[a,e,f,h,1]

Departments of [a]Earth and Space Sciences and [e]Atmospheric and Oceanic Sciences, [f]Institute of the Environment and Sustainability, and [h]California NanoSystems Institute, University of California, Los Angeles, CA 90095; [b]Division of Geological and Planetary Sciences, California Institute of Technology, Pasadena, CA 91125; [c]Department of Atmospheric and Oceanic Sciences, University of Colorado, Boulder, CO 80303; [d]Laboratoire de Météorologie Dynamique, Institut Pierre Simon LaPlace, Centre National de la Recherche Scientifique, 75252 Paris Cedex 05, France; and [g]Ministry of Education Key Laboratory of Surficial Geochemistry, Department of Earth Sciences, Nanjing University, 163 Xianlindadao, Nanjing 210046, China

Edited by Thure E. Cerling, University of Utah, Salt Lake City, UT, and approved April 18, 2013 (received for review August 2, 2012)

The East Asian monsoon is one of Earth's most significant climatic phenomena, and numerous paleoclimate archives have revealed that it exhibits variations on orbital and suborbital time scales. Quantitative constraints on the climate changes associated with these past variations are limited, yet are needed to constrain sensitivity of the region to changes in greenhouse gas levels. Here, we show central China is a region that experienced a much larger temperature change since the Last Glacial Maximum than typically simulated by climate models. We applied clumped isotope thermometry to carbonates from the central Chinese Loess Plateau to reconstruct temperature and water isotope shifts from the Last Glacial Maximum to present. We find a summertime temperature change of 6–7 °C that is reproduced by climate model simulations presented here. Proxy data reveal evidence for a shift to lighter isotopic composition of meteoric waters in glacial times, which is also captured by our model. Analysis of model outputs suggests that glacial cooling over continental China is significantly amplified by the influence of stationary waves, which, in turn, are enhanced by continental ice sheets. These results not only support high regional climate sensitivity in Central China but highlight the fundamental role of planetary-scale atmospheric dynamics in the sensitivity of regional climates to continental glaciation, changing greenhouse gas levels, and insolation.

A wide range of archives, including speleothem, marine, lake, Himalayan glacier ice core, and loess sediment records, have shown that monsoons exhibit significant variations on orbital and suborbital time scales (e.g., refs. 1–11). Perhaps most compelling are precisely dated speleothem records that show glacial–interglacial fluctuations in carbonate $^{18}O/^{16}O$ ratios ($\delta^{18}O$) of up to 6‰ and can also resolve abrupt responses that are coherent with those recorded in Greenland ice cores, indicating a close coupling of changes in the East Asian Monsoon and the climate of the North Atlantic (1–3). Although speleothem and other monsoonal proxy records show a striking concordance, it is not precisely clear to what extent these archives quantitatively reflect changes in temperature or other processes. In carbonate $\delta^{18}O$ records, for example, there are possible contributions of temperature, precipitation at the site or along air mass trajectories, an altered balance between winter and summer monsoon intensity, changing frontal systems and water vapor sources, humidity effects, and kinetic isotope fractionations (1, 12–15). Therefore, quantitative constraints on terrestrial climate changes from thermodynamically based proxies are limited, yet are crucial for constraining the sensitivity of this region and others to future climate forcing (16, 17).

Here, we provide direct quantitative determinations of changes in temperature and water $\delta^{18}O$ from the Last Glacial Maximum (LGM) to the present using a recently developed proxy and examine the mechanisms that may be responsible for these changes with a series of general circulation models (GCMs) with both standard and high resolution. We utilize clumped isotope thermometry to estimate temperatures and precipitation $\delta^{18}O$, an approach that is based on the thermodynamic preference of ^{13}C and ^{18}O to bond to each other or "clump" in a carbonate mineral (18, 19). ^{13}C-^{18}O bonding is related to temperature but not to the bulk isotopic composition of the fluid from which a mineral precipitates (18, 19). In practice, the parameter that is measured is the Δ_{47} value of CO_2 gas liberated on phosphoric acid digestion of carbonate minerals, a measure of ^{13}C-^{18}O bond excess in a sample relative to what should be present if isotopes were stochastically distributed (*SI Appendix*). Because carbonate $\delta^{18}O$ is also measured as part of the clumped isotope analysis, we are able to calculate the $\delta^{18}O$ of the water from which the carbonate grew and deconvolve changes in meteoric water $\delta^{18}O$.

Results and Discussion

We analyzed calcitic soil nodules and aragonitic shells of *Cathaica* sp. (*SI Appendix*, Fig. S2) recovered from both modern and LGM strata (L1.LL1) from the Chinese Loess Plateau at Puxian in Shanxi Province (36.421° N, 111.147° E, 1,148-m elevation; *SI Appendix*). We report clumped isotope measurements on 32 modern, and 37 LGM gastropod specimens and nine glacial soil nodules, as well as a small number of analyses on modern/recent soil carbonate to complement the study of modern soil carbonates by Passey et al. (20). The large number of gastropod specimens we have analyzed is important to establishing glacial–interglacial changes because *Cathaica* sp. are short-lived; thus, each individual may present a selectively biased sample of seasonally varying climate. Therefore, these data must be averaged over many individuals to arrive at a meaningful population average. On the other hand, because individual gastropods sample climate over a much shorter time scale than large nodular soil carbonates, variability in this dataset may shed light on seasonal and other short-time-scale climatic variations (*SI Appendix*, Figs. S6 and S7 and Tables S1–S3).

Pedogenic carbonates are generally thought to form predominantly in the warm summer months (*SI Appendix*), and both a recent calibration study (20) and our own data show that soil carbonate Δ_{47}-temperatures correlate well with warm-month average temperatures (*SI Appendix*, Fig. S4). Average Δ_{47}-derived temperatures from modern gastropod specimens from Puxian

Author contributions: R.A.E., C.R., and A.K.T. designed research; R.A.E., C.R., and A.K.T. performed research; G.L. contributed new reagents/analytic tools; R.A.E., C.R., J.L.M., J.M.E., U.S., and J.D.N. analyzed data; and R.A.E. wrote the paper.

The authors declare no conflict of interest.

This article is a PNAS Direct Submission.

[1]To whom correspondence may be addressed. E-mail: rob.eagle@gmail.com or aradhna.tripati@gmail.com.

This article contains supporting information online at www.pnas.org/lookup/suppl/doi:10.1073/pnas.1213366110/-/DCSupplemental.

(Table 1 and *SI Appendix*, Figs. S6 and S7) correlate with warm-month average daily high temperatures, which are also the wettest and most humid months (*SI Appendix*, Fig. S5) and presumably reflect the predominant season of growth for *Cathaica* sp. (*SI Appendix*). In-depth calibration studies of ^{13}C-^{18}O bonding in biologically precipitated carbonates and carbonate-containing minerals, including foraminifera, coccoliths, teeth, terrestrial gastropods, and some corals, have shown that at least in some materials that show nonequilibrium "vital" effects in $\delta^{18}O$ of up to 4‰, measured Δ_{47} values are indistinguishable from inorganic calcite (21–24). No significant differences between calcite and aragonite formed at the same temperature were observed (21, 23). In a calibration study of terrestrial gastropod shells, Zaarur et al. (24) find that Δ_{47} values from diverse taxa and localities do not conform to a universal relationship with temperatures during presumed gastropod activity seasons. However, in a subset of their data from localities with climates most similar to monsoonal regions (i.e., warm, wet summers), their data do show correlation with summertime temperatures, with gastropod Δ_{47}-derived calcification temperatures most similar to average summertime high temperatures (*SI Appendix*, Fig. S6), a similar observation to our data from Puxian and indicating an affinity of warm temperature for optimum growth (a description of proxy systematics is provided in *SI Appendix*).

We find that average temperatures from glacial soil nodules and gastropods were ∼6–7 °C cooler than modern temperatures (Table 1 and *SI Appendix*, Table S1); therefore, the amplitude of wintertime temperature change (and mean annual temperature change) is likely to be even greater. It seems reasonable to suppose that in the case of gastropods, the temperature difference is a contrast between summer highs. It is possible that a change in timing of precipitation could have contributed to a shift in the seasonality of gastropod growth; however, we consider this unlikely due to the apparent affinity to warm temperatures for optimum growth of *Cathaica* sp. Ultimately, the broad agreement between the temperature change indicated by soil carbonates (taken to indicate warm-month mean temperatures) and that indicated by gastropods, which are within 1 SE of each other, lends confidence to our conclusions.

We note that the summertime temperature changes we reconstruct are consistent with constraints on the elevation of the July freezing line in central and north China from snowline depressions, which exhibit large shifts from the LGM to the present, although these indicators are also influenced by changes in atmospheric processes (25, 26). Empirical proxies, including pollen and phytolith assemblages, permafrost extents, and lipid distributions, have suggested that temperature changes from the LGM to the present in central China yield variable results ranging from as little as 4 °C to as much as 13 °C (25, 27–30), and often have an uncertain seasonal bias. The importance of the clumped isotope data we present is that it provides a direct thermodynamically based estimate that can be relatively confidently assigned to a change in summertime temperatures. Our measurements are also important in that they permit us to deconvolve temperature and changes in the $\delta^{18}O$ of meteoric water with confidence using stable isotopic equilibria and based on measurements of a single material. The large degree of midlatitude continental cooling we reconstruct is consistent with evidence for significant cooling in the tropics from snowline reconstructions and foraminiferal Mg/Ca ratios at the LGM (31, 32) associated with reduced greenhouse gases and increased snow and ice cover, in light of evidence that cooling may have been

Table 1. Modern climatological data and proxy based reconstructions of past climate

Climate parameter	Value
Modern warm month (JJA) climatological data	
Monthly average*	23.3 °C
Monthly average daily high*	28.8 °C
GNIP station† water isotopes in precipitation (V-SMOW)	−7.1‰
Pedogenic carbonate-derived temperature and $\delta^{18}O$	
LGM temperature (soil carbonate Δ_{47}-derived)‡	17.8 ± 2.0 °C
LGM soil carbonate formation water $\delta^{18}O$ (ice-vol. corr.)§	−9.1 ± 0.5‰
ΔT (LGM-GNIP station)¶	−5.5 ± 2.0 °C
$\Delta\delta^{18}O$ (soil carbonate-GNIP station water $\delta^{18}O$; V-SMOW)‖	−2.0 ± 0.5‰
Terrestrial gastropod calcification temperature and $\delta^{18}O$	
Modern temperature (Δ_{47}-derived)	31.2 ± 1.5 °C
LGM temperature (Δ_{47}-derived)	24.2 ± 1.9 °C
Modern body water $\delta^{18}O$ (V-SMOW)	−0.5‰
Glacial body water $\delta^{18}O$ (ice-vol. corr.; V-SMOW)	−5.5‰
ΔT (LGM-modern)	−7.0 ± 2.4 °C
$\Delta\delta^{18}O$ meteoric water (LGM-modern; V-SMOW)**	−5.2 ± 0.5‰

Values with a ± symbol indicate two SE values derived from the error in stable isotope determinations or the propagated uncertainty when comparing two values with errors. JJA, June, July, August; V-SMOW, Vienna standard mean ocean water.

*Data compiled for the years 2007–2010 from the nearby climate station at Yan An, Shaanxi province (36.6° N, 109.5° E, 959-m elevation); details are provided in *SI Appendix*.

†Data from the nearby Taiyuan Global Network for Isotope Precipitation (GNIP) station (37.8° N, 112.6° E, 778-m elevation), which has the most similar altitude to Puxian of the GNIP sites in closest proximity to our study site (*SI Appendix*, Table S8).

‡Δ_{47}-Derived temperatures are determined from the stable isotope data given in *SI Appendix*, Tables S1–S3.

§Calculated using the Δ_{47}-derived temperature and soil carbonate $\delta^{18}O$ and corrected by 1.2‰ for LGM ice volume change.

¶Error calculated using a 0.5 °C uncertainty in modern climatological data and the error in the LGM Δ_{47} temperature determination.

‖Error is the propagated error of temperature and $\delta^{18}O$ determinations (*SI Appendix*).

**Calculated using an isotope flux model of gastropod body water and assuming constant humidity in gastropod microenvironment; details are provided in *SI Appendix*.

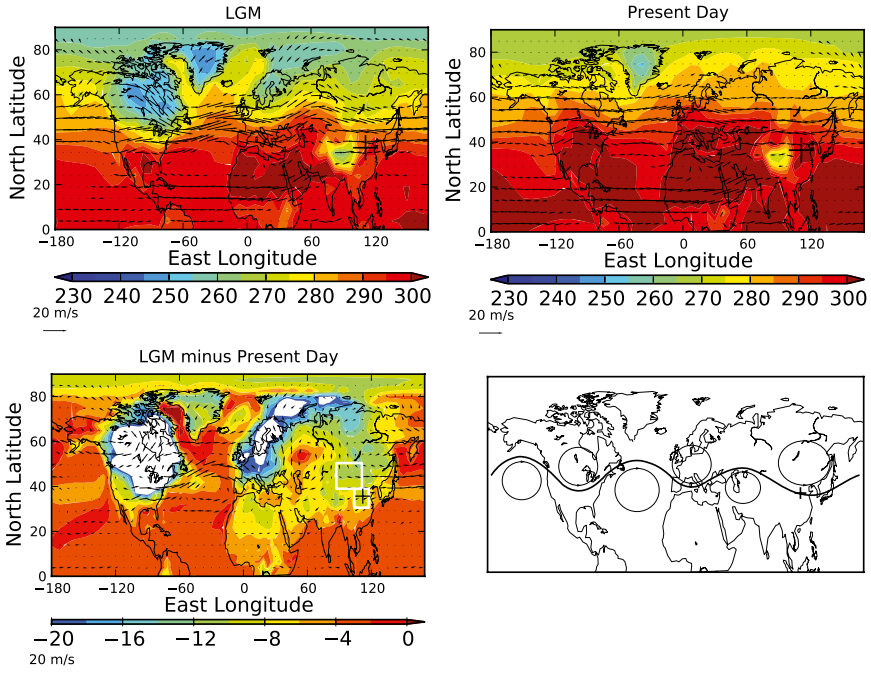

Fig. 1. Northern hemisphere climates simulated using the LMDZ4 model. Summer (June, July, August) surface temperatures (colors) and midlevel winds (arrows; at 500 hPa) determined from LMDZ4 simulations of the LGM show not only general cooling of the high-latitude Northern Hemisphere (*Upper Left*) but regional enhancements or reductions in cooling of midlatitudes due to the presence of stationary waves (*Lower Right*, schematic), as indicated in the anomalies in these fields (*Lower Left*; white regions are simulated to have more than 20 °C cooling) relative to a present-day LMDZ4 simulation (*Upper Right*). Northwesterly winds at Puxian (marked with a cross) associated with the stationary wave pattern in the LGM simulation enhance the simulated cooling by ∼30% relative to a simulation with the stationary waves suppressed (by removing the continental ice sheets; *SI Appendix*, Fig. S9). The winds associated with the stationary wave pattern also are responsible for a simulated light water isotope signal at Puxian, as observed (Fig. 3). Color bars represent either temperature (degrees Kelvin) or temperature change. (*Lower Left*) White boxes indicate ranges of averaging for our diagnostics in Fig. 2.

generally amplified on a global basis at higher latitudes in terrestrial settings (33).

Most GCMs that were used in the Paleoclimate Modeling Intercomparison Project, Phase 2 (PMIP2) study typically show ∼2–3 °C of summer cooling at Puxian (Figs. 1 and 2 and *SI Appendix*, Table S5) and similar or slightly larger changes in annual temperatures (i.e., reflecting greater change in winter temperatures). We suggest that a significant factor in the systematic underestimations of temperature changes in the region by most climate models between most of the GCMs and our proxy data stems from the inability of some models to simulate the stationary wave response to continental ice sheets. Puxian is located in a region with a strong gradient in the stationary wave temperature response (Fig. 1), and is thus is well placed to distinguish among models. Only two PMIP2 models simulated a temperature change that approached our proxy data (Fig. 2), and these models both exhibit a much more pronounced and southward-shifted cyclonic circulation at the LGM in northern Asia that is responsible for the advection of cool air from the north toward the Loess Plateau (*SI Appendix*, Fig. S3). We also present a unique set of low- and high-resolution simulations (*SI Appendix*) with the Laboratoire de Météorologie Dynamique-Zoom 4 (LMDZ4) model, which both show a strong stationary wave response. These models simulate temperatures that were 8.8 °C and 6.7 °C cooler at the LGM, respectively (Figs. 1 and 2).

Stationary waves are forced by land–sea contrast, topography, and ice sheets, although the response depends significantly on model zonal-mean winds. To identify the contribution of ice sheets, we ran a series of LGM simulations with and without continental ice sheets (Fig. 2 and *SI Appendix*, Fig. S9). Fig. 1 demonstrates the influence of the ice sheets at the LGM on stationary waves, which are tightly correlated with strong surface temperature gradients as required by thermal wind balance. Southward deflections in the jet stream bring cold air toward the equator, and vice versa, creating an alternating enhanced/reduced cooling pattern in the temperature change between the LGM and the present (Fig. 1). North of the study site, a counterclockwise circulating stationary pattern advects cold air from the northwest, resulting in greater cooling. In our simulation with the ice sheets removed, the LGM stationary wave pattern is not enhanced relative to the present; as a result, the simulated cooling at the study site is reduced. In this particular model simulation, the response to continental ice sheets accounts for an ∼30% enhancement in the cooling simulated by our model at Puxian.

We also investigated changes in the isotopic composition of meteoric waters since the LGM. Both soil carbonates and gastropods support a shift toward lower values of the $\delta^{18}O$ of water during the LGM compared with the present at Puxian; soil carbonates indicate a change of 2‰, and gastropods indicate a change of 5‰. Whereas soil carbonates are likely to be a more passive tracer of meteoric water compositions (34), evaporative enrichment of gastropod body water likely leads to increases in $\delta^{18}O$ relative to meteoric water (35) over the short lifespan of the organism, similar to that observed in plants (details are provided in *SI Appendix*). For our purposes, the crucial result is that we are able to deconvolve the influence of temperature to calculate meteoric water composition changes since the LGM from a single thermodynamically based measurement and, despite uncertainties in proxy systematics, place reasonable constraints on its magnitude, allowing us to validate our climate model simulations.

Both our low-resolution and high-resolution simulations are isotope-enabled; thus, they also allow us both to validate our model output with our proxy data and to interrogate the driving force of the water isotope signal. We hypothesized higher resolution might be required to simulate isotope signals faithfully in regions with strong humidity gradients, as is the case in monsoonal

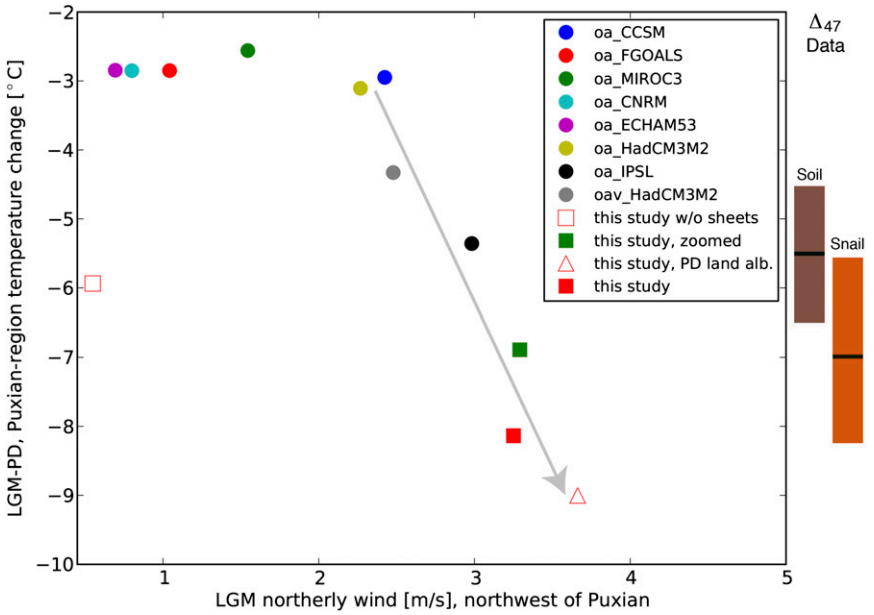

Fig. 2. PMIP2 simulations of LGM (circles) and our simulations with the LMDZ4 model (squares and triangle) show a correspondence between LGM-present day (PD) cooling in the Puxian region (averaged over 30–40° N latitude and 105–115° E longitude) and a diagnostic of the stationary wave to the Northwest of this region [500-hPa northerly winds averaged over 40–50° N latitude and 80–110° E longitude; white boxes in Fig. 1 (*Lower Left*) show averaging regions]. PMIP2 models with weak stationary waves (<2.5-m/s northerly winds) simulate −3 °C cooling, which is inconsistent with our data. Models that simulate stronger stationary waves (>2.5-m/s northerly winds) also show enhanced cooling of the Puxian region. Our simulations with the LMDZ4 model (squares and triangle) show enhanced northerly winds and substantially more cooling at Puxian along the same trend as the PMIP2 models. If the stationary waves are artificially suppressed in the LMDZ4 model [by removing the continental ice sheets (open red square); *SI Appendix*, Fig. S9], the simulated cooling is reduced by ∼30% relative to the LMDZ4 simulation at the same resolution (filled red square). Proxy data are indicated by black bars to the right of the plot, with filled brown and orange areas representing 1 SE of the temperature change determined from soil carbonates and gastropods, respectively. The ensemble of models demonstrates enhanced regional LGM climate sensitivity (represented by the gray arrow) in East Asia correlated with the far-field influence of continental ice sheets on the global stationary wave pattern. alb., albedo; oa, ocean atmosphere enabled model; oav, ocean, atmosphere, and vegetation; oa_CCSM, community climate system model; oa_CNRM, Centre National de Recherches Météorologiques; oa_ECHAM53, Max-Planck-Institut für Meteorologie General Circulation Model 5; oa_FGOALS, Institute of Atmospheric Physics, Chinese Academy of Sciences Model; oa_IPSL, Institut Pierre Simon Laplace; oa_MIROC3, Atmosphere and Ocean Research Institute (University of Tokyo), National Institute for Environmental Studies, and Japan Agency for Marine-Earth Science and Technology; oa_HadCM3M2, Met Office Hadley Centre.

climates, because specific humidity is a quasiconserved tracer of the atmospheric flow (unlike temperature, which is smoothed at the deformation scale by the influence of gravity wave radiation). The standard-resolution model simulates a $\delta^{18}O$ change of −2‰, whereas the high-resolution simulations produce a $\delta^{18}O$ change of −3.6‰ (after correcting for seawater change). Although both models simulate lighter precipitation of $\delta^{18}O$ during the LGM in the region, and similar magnitude changes to what is inferred from the proxy data, the global simulation with enhanced resolution over Asia further indicates that fine-scale dynamic phenomena may be essential in setting the isotope signal in the region (Fig. 3 and *SI Appendix*), and thus will be an important consideration when comparing our data with published results from speleothems and other archives from different sites in Asia. If the temperature changes we reconstruct at Puxian can be extrapolated to speleothem sites, as our model output suggests may be the case (*SI Appendix*, Table S9), our data would call for a greater temperature component to the speleothem records than commonly assumed (e.g., ref. 1). For example, a temperature change of 7 °C would translate into an ∼1.75‰ change in speleothem carbonate $\delta^{18}O$ from the LGM to the late Holocene. However, there are substantial uncertainties in doing this; for example, the Dongge and Hulu speleothem sites are located 5–11° south of Puxian, and it is possible the LMDZ4 model may not completely capture gradients in temperature that could exist between our site and the cave sites. Additionally, our proxy temperature determinations are recording warm-month temperatures in surface and shallow soil environments. Therefore, if the caves in which speleothems formed were buffered from temperature changes at the surface, or if speleothems formed at different times of the year, the temperature component of the speleothem record could be different from our reconstruction. Clearly, important follow-up work to our study will be to reconstruct gradients of temperature and water $\delta^{18}O$ in the region using the clumped isotope approach.

Conclusions

Our data represent a robust estimate of LGM-recent temperature changes for central China that is well placed to discriminate among model simulations of the regional sensitivity pattern. The large temperature changes we reconstruct are reproduced in our simulations, which indicate significant cooling and lighter rainfall isotope compositions across most of central Asia, and changes in surface relative humidity over the Chinese Loess Plateau. This work allows us to provide a robust estimate of LGM-recent temperature changes for central China that is well placed to discriminate among model simulations of the regional sensitivity pattern. The changes in temperature patterns from the LGM to the present reflect the far-field influence of North American and European ice sheets on the stationary wave pattern in midlatitudes. Our results imply that the regional climate in East Asia is more sensitive to continental glaciation, insolation, and greenhouse gas forcing at the LGM than most global climate models indicate.

Methods

Samples. Thirty-two modern terrestrial gastropod snail shells were collected from the Chinese Loess Plateau at Puxian in Shanxi Province (*SI Appendix*, Figs. S1 and S2; 36.421° N, 111.147° E, 1,148 m). Modern snails were collected

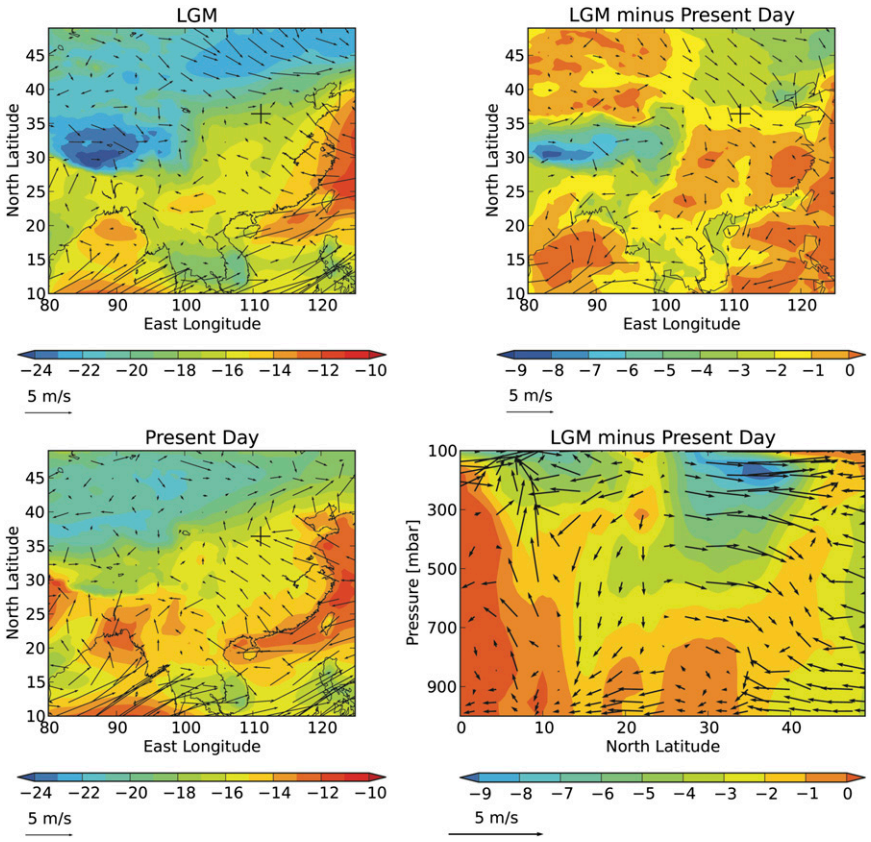

Fig. 3. June, July, August water vapor oxygen isotope signal [Vienna standard mean ocean water (V-SMOW)] simulated in East Asia by the LMDZ4 model (colors; $\delta^{18}O$ in per mil) and surface winds (arrows) under LGM forcing (*Upper Left*) indicate the presence of an ^{18}O-depleted region to the northwest of Puxian (marked with a cross) and a strong cross-gradient northwesterly surface flow transporting the depleted air to Puxian. The anomalies of these fields (*Upper Right*) relative to a present-day simulation (*Lower Left*) highlight the enhanced northwesterly winds at Puxian associated with the large-scale stationary wave pattern described in Fig. 1. Latitude-pressure cross-sections of $\delta^{18}O$ and winds averaged in longitude over the Puxian region (105–115° E longitude; *Lower Right*) show the coincidence between northerly winds and a light isotope signal near the surface at Puxian (36.4° N latitude). This dynamic feature indicates that the stationary wave over East Asia halts the northward advance of the East Asian Monsoon, keeping the Puxian region relatively cold and dry in the LGM.

on the surface of the Loess Plateau. Individuals that recently died can be identified by the colorful organic coating (banding) on the shells. Specimens were identified as *Cathaica* sp., as shown in *SI Appendix*, Fig. S2, and have an aragonitic mineralogy. Field observations show that snails are active only during the rainy season. Thirty-seven shells and pedogenic soil carbonate nodules from the same site were selected from loess stratigraphic unit L1. LL1, which has been extensively described and is known to correspond to the LGM (36, 37). Individual gastropod shells were first cleaned with a course-grained paintbrush to remove large fragments of soil and/or organic material. Shells were gently crushed to produce large fragments and then were sonicated and washed 6 to 10 times in deionized water, a procedure that produced very clean shell material free from any macroscopic contaminants. Shell material was then dried at 50 °C overnight and crushed into a fine powder with a pestle and mortar. A more detailed description of the samples and geological setting is provided in *SI Appendix*.

Δ_{47} Measurements of Carbonates. Approximately 8- to 12-mg samples of calcium carbonate were reacted for 20 min at 90 °C on an online common phosphoric acid bath system described previously (20). CO_2 gas was immediately frozen by means of liquid nitrogen, after passing through a dry ice/ethanol trap. Cryogenic purification of CO_2 was achieved using an automated online vacuum line, as described previously (38). $\delta^{13}C$, $\delta^{18}O$, Δ_{47}, and Δ_{48} in CO_2 derived from the phosphoric acid digestion of carbonates were determined using a Thermo Scientific MAT 253 gas-source mass spectrometer utilizing published configuration and methods (20, 38). Because sample reactions were carried out at 90 °C, rather than 25 °C as in the study by Ghosh et al. (18), we applied the empirically derived acid digestion fractionation correction of 0.08‰ for Δ_{47} values reported by Passey et al. (20). The vast majority of data presented here were collected before the proposition of the analysis of CO_2 equilibrated with water of known temperatures to define an absolute reference frame for Δ_{47} measurements; thus, we present data in both the reference frame defined by Ghosh et al. (18) and in the absolute reference frame proposed by Dennis et al. (39) by using a transfer function based on accepted standard values (*SI Appendix*, Tables S1–S3). For converting Δ_{47} values into calcification temperatures, we continued to use the equation defined by Ghosh et al. (18): $\Delta_{47} = 0.0592\ (10^6 \cdot T^{-2}) - 0.02$. A more detailed description of analytical methods and calculations is provided in *SI Appendix*.

Model Output and Analysis. The primary numerical simulations presented here were with the LMDZ4 GCM, the atmospheric component of the coupled model of the Institut Pierre-Simon Laplace (40)*. The LMDZ4 GCM has the capability for both standard-resolution and high-resolution isotope-enabled simulations. In the high-resolution LMDZ4 model, the grid can be stretched in such a way so as to increase the resolution in a region of interest down to a few tens of kilometers and to decrease the resolution everywhere else. The LMDZ4 GCM can thus be used as a regional model. The major difference from a regional model is that the simulations remain global, such that the benefits of the high resolution on the large-scale circulation and the vapor isotopic composition can feed back on the global simulation. Proxy data and model outputs were also compared with GCMs from the PMIP2 database (41). More detailed information on models and analysis is provided in *SI Appendix*.

*Marti O, et al. (2005) The new IPSL climate system model. *Tech Rep, IPSLCM4, IPSL*.

ACKNOWLEDGMENTS. We thank D. Battisti, M. Berkelhammer, J.-E. Lee, A. LeGrande, F. Pausata, and C. Yapp for valuable discussions during the formulation of this paper. We thank J. Canet, M. Enriquez, and J. Meyerson (University of California, Los Angeles) for the extraction of Climate Station and PMIP2 model data, and D. Pittman for supervising the data extraction. We acknowledge the international modeling groups participating in the PMIP2 for providing their results for analysis, and the Laboratoire des Sciences du Climat et l'Environnement (LSCE) for collecting and archiving the model results. We also thank N. Thiagarajan for provision of a compilation of speleothem isotope data. This work was funded by National Science Foundation (NSF) Grant EAR-0949191 (to A.K.T.) as well as by NSF Grants EAR-0909194 and EAR-1024929 (to J.M.E.). J.D.N. was supported by NSF Grant AGS-1102838. This work was also supported by National Aeronautics and Space Administration Grant 07-NEWS07-0020 (to D. Noone, which supported C.R.).

1. Wang YJ, et al. (2001) A high-resolution absolute-dated late Pleistocene Monsoon record from Hulu Cave, China. *Science* 294(5550):2345–2348.
2. Yuan D, et al. (2004) Timing, duration, and transitions of the last interglacial Asian monsoon. *Science* 304(5670):575–578.
3. Wang Y, et al. (2008) Millennial- and orbital-scale changes in the East Asian monsoon over the past 224,000 years. *Nature* 451(7182):1090–1093.
4. Heller F, Liu T-S (1982) Magnetostratigraphical dating of loess deposits in China. *Nature* 300:431–433.
5. Clemens S, Prell W, Murray D, Shimmield G, Weedon G (1991) Forcing mechanisms of the Indian Ocean monsoon. *Nature* 353:720–725.
6. Rea DK (1994) The paleoclimatic record provided by eolian deposition in the deep sea: The geologic history of wind. *Rev Geophys* 32:159–195.
7. Porter SC (2001) Chinese loess record of monsoon climate during the last glacial-interglacial cycle. *Earth-Science Reviews* 54:115–128.
8. Porter S, An Z (1995) Correlation between climate events in the North Atlantic and China during the last glaciations. *Nature* 375:305–308.
9. Liu T, Ding ZL (1998) Chinese loess and the paleomonsoon. *Annu Rev Earth Planet Sci* 26:111–145.
10. An Z (2000) The history and variability of the East Asian paleomonsoon climate. *Quat Sci Rev* 19:171–187.
11. Thompson LG, et al. (1997) Tropical climate instability: The last glacial cycle from a Qinghai-Tibetan ice core. *Science* 276:1821–1825.
12. Johnson KR, Ingram BL, Sharp WD, Zhang PZ (2006) East Asian summer monsoon variability during Marine Isotope Stage 5 based on speleothem delta O-18 records from Wanxiang Cave, central China. *Palaeogeogr Palaeoclimatol Palaeoecol* 236: 5–19.
13. Dayem KE, Molnar P, Battisti DS, Roe GH (2010) Lessons learned from oxygen isotopes in modern precipitation applied to interpretation of speleothem records of paleoclimate from eastern Asia. *Earth Planet Sci Lett* 295:219–230.
14. Pausata FR, Battisti DS, Nisancioglu KH, Bitz CM (2011) Chinese stalagmite $\delta^{18}O$ controlled by changes in the Indian monsoon during a simulated Heinrich event. *Nat Geosci* 4:474–480.
15. Affek HP, Bar-Matthews M, Ayalon A, Mathews A, Eiler JM (2008) Glacial/interglacial temperature variations in Soreq cave speleothems as recorded by 'clumped isotope' thermometry. *Geochim Cosmochim Acta* 72(22):5351–5360.
16. Schmittner A, et al. (2011) Climate sensitivity estimated from temperature reconstructions of the Last Glacial Maximum. *Science* 334(6061):1385–1388.
17. Hegerl GC, Russon T (2011) Climate change. Using the past to predict the future? *Science* 334(6061):1360–1361.
18. Ghosh P, et al. (2006) ^{13}C-^{18}O bonds in carbonate minerals: A new kind of paleothermometer. *Geochim Cosmochim Acta* 70(6):1439–1456.
19. Schauble EA, Ghosh P, Eiler JM (2006) Preferential formation of ^{13}C-^{18}O bonds in carbonate minerals, estimated using first-principles lattice dynamics. *Geochim Cosmochim Acta* 70(10):2510–2529.
20. Passey BH, Levin NE, Cerling TE, Brown FH, Eiler JM (2010) High-temperature environments of human evolution in East Africa based on bond ordering in paleosol carbonates. *Proc Natl Acad Sci USA* 107(25):11245–11249.
21. Tripati AK, et al. (2010) ^{13}C-^{18}O isotope signatures and 'clumped isotope' thermometry in foraminifera and coccoliths. *Geochim Cosmochim Acta* 74(20):5697–5717.
22. Eagle RA, et al. (2010) Body temperatures of modern and extinct vertebrates from ^{13}C-^{18}O bond abundances in bioapatite. *Proc Natl Acad Sci USA* 107(23):10377–10382.
23. Thiagarajan N, Adkins J, Eiler J (2011) Carbonate clumped isotope thermometry of deep-sea corals and implications for vital effects. *Geochim Cosmochim Acta* 75: 4416–4425.
24. Zaarur S, Olack G, Affek HP (2011) Paleo-environmental implication of clumped isotopes in land snail shells. *Geochim Cosmochim Acta* 75(22):6859–6869.
25. Zhuo Z, Baoyin Y, Petit-Maire N (1998) Paleoenvironments in China during the Last Glacial Maximum and the Holocene Optimum. *Episodes* 21(3):152–158.
26. Rost KT (2000) Pleistocene paleoenvironmental changes in the high mountain ranges of central China and adjacent regions. *Quat Int* 65/66:147–160.
27. Sun X, Song C, Wang F, Sun M (1997) Vegetation history of the Loess Plateau of China during the last 100,000 years based on pollen data. *Quat Int* 37:25–36.
28. Cui Z, Yang J, Zhang W, Zhao L, Xie Y (2004) Discovery of a large area of ice-wedge networks in Ordos: Implications for the southern boundary of permafrost in the north of China as well as for the environment in the latest 20 kaBP. *Chin Sci Bull* 49: 1177–1184.
29. Lu H-Y, Wu N-Q, Liu K-B, Jiang H, Liu T-S (2007) Phytoliths as quantitative indicators for the reconstruction of past environmental conditions in China II: Paleoenvironmental reconstruction in the Loess Plateau. *Quat Sci Rev* 26:759–772.
30. Peterse F, et al. (2011) Decoupled warming and monsoon precipitation in East Asia over the last deglaciation. *Earth Planet Sci Lett* 301:256–264.
31. Porter SC (2000) Snowline depression in the tropics during the Last Glaciation. *Quat Sci Rev* 20:1067–1091.
32. Lea DW, Pak DK, Spero HJ (2000) Climate impact of late quaternary equatorial pacific sea surface temperature variations. *Science* 289(5485):1719–1724.
33. Shakun JD, Carlson AE (2010) A global perspective on Last Glacial Maximum to Holocene climate change. *Quat Sci Rev* 29:1801–1816.
34. Cerling TE (1984) The stable isotopic composition of modern soil carbonate and its relationship to climate. *Earth Planet Sci Lett* 71(2):229–240.
35. Balakrishnan M, Yapp CJ (2004) Flux balance models for the oxygen and carbon isotope compositions of land snail shells. *Geochim Cosmochim Acta* 68(9):2007–2024.
36. Kukla G, An Z (1989) Loess stratigraphy in central China. *Palaeogeogr Palaeoclimatol Palaeoecol* 72:203–225.
37. Ding ZL, et al. (2002) Stacked 2.6-Ma grain size record from the Chinese loess based on five sections and correlation with the deep-sea $\delta^{18}O$ record. *Paleoceanography*, 10.1029/2001PA000725.
38. Huntington KW, et al. (2009) Methods and limitations of 'clumped' CO_2 isotope (Delta47) analysis by gas-source isotope ratio mass spectrometry. *J Mass Spectrom* 44(9):1318–1329.
39. Dennis KJ, Affek HP, Passey BH, Schrag DP, Eiler JM (2011) Defining an absolute reference frame for 'clumped' isotope studies of CO_2. *Geochim Cosmochim Acta* 75: 7117–7131.
40. Hourdin F, et al. (2006) The LMDZ4 general circulation model: Climate performance and sensitivity to parametrized physics with emphasis on tropical convection. *Climate Dynamics* 27:787–813.
41. Braconnot P, et al. (2007) Results of PMIP2 coupled simulations of the Mid-Holocene and Last Glacial Maximum—Part 1: Experiments and large-scale features. *Climate of the Past* 3:261–277.